

# Numerical Study of the Incommensurate Phase in Spin-Peierls Systems

A. E. Feiguin, J. A. Riera, A. Dobry and H. A. Ceccatto

*Instituto de Física Rosario, Boulevard 27 de Febrero 210 bis, 2000 Rosario, Argentina*

We analyze several properties of the lattice solitons in the incommensurate phase of spin-Peierls systems using exact diagonalization and quantum Monte Carlo. These systems are modelled by an antiferromagnetic Heisenberg chain with nearest and next-nearest neighbor interactions coupled to the lattice in the adiabatic approximation. Several relations among features of the solitons and magnetic properties of the system have been determined and compared with analytical predictions. We have studied in particular the relation between the soliton width and the spin-Peierls gap. Although this relation has the form predicted by bosonized field theories, we have found some important quantitative differences which could be relevant to describe experimental studies of spin-Peierls materials.

PACS numbers: 74.20.-z, 74.20.Mn, 74.25.Dw

## I. INTRODUCTION

One-dimensional or quasi-one-dimensional magnetic systems show many fascinating properties which continue to attract an intense theoretical activity. One of these properties is the presence of a spin gap in antiferromagnetic Heisenberg chains with integer spin<sup>1</sup> and in ladders.<sup>2</sup> Another, particularly complex, system which presents a spin gap is the spin-Peierls (SP) system. In this system a Heisenberg chain coupled to the lattice presents an instability at a critical temperature,  $T_{SP}$ , below which a dimerized lattice pattern appears and a spin gap opens in the excitation spectrum.<sup>3</sup>

The interest in the spin-Peierls phenomena was recently revived after the first inorganic SP compound,  $\text{CuGeO}_3$ , was found.<sup>4</sup> This inorganic material allows the preparation of better samples than the organic SP compounds and hence several experimental techniques can be applied to characterize the properties of this system.<sup>5</sup> Besides, this compound can be easily doped with magnetic and non-magnetic impurities, leading to a better understanding of its ground state and excitations.<sup>6</sup>

Spin-Peierls systems present also a very rich and interesting behavior in the presence of an external magnetic field. Below the spin-Peierls transition temperature, and for magnetic fields  $H$  smaller than a critical value  $H_{cr}(T)$ , the system is in its spin-Peierls phase, characterized by a gapped nonmagnetic ( $S^z = 0$ ) ground state with a dimerized pattern or alternating nearest-neighbor (NN) interactions. For  $T < T_{tc} < T_{SP}$ , at  $H = H_{cr}(T)$  a transition occurs from the dimerized phase to a gapless incommensurate (IC) state characterized by a finite magnetization,  $S^z > 0$ .  $T_{tc}$  is the temperature of the point at which the dimerized, incommensurate and uniform phases meet. The dimerized-IC transition was predicted by some theories<sup>7</sup> to be of first order at low temperatures, and this is the behavior found in experimental studies<sup>8,9</sup>. Other theories predict that this transition is a second order one.<sup>10</sup>

A simple picture of the dimerized-IC transition can be

obtained by mapping the Heisenberg spin chain to a spinless fermion system by a Jordan-Wigner transformation. The effect of the magnetic field favoring a nonzero  $S^z$  due to the Zeeman energy can be interpreted as a change in the band filling of the equivalent spinless fermion system. As a result, the momentum of the lattice distortion moves away from  $\pi$  as  $\tilde{q} = (1 - S^z/N)\pi$ , where  $N$  is the number of sites on the chain. However, since *umklapp* processes pin the momentum at  $\pi$  up to a critical field  $H_{cr}(T)$ , the lattice distortion will remain a simple dimerization and the magnetic ground state will remain a singlet.<sup>11</sup> Theoretical<sup>10,12,13</sup> and experimental<sup>14,15</sup> studies indicate that the lattice distortion pattern in the IC phase corresponds to an array of solitons. A complementary picture indicating how a soliton lattice could appear as a consequence of the finite magnetization in the IC phase is the following. Let's assume that the dominant contribution to the magnetic ground state comes from a state of NN singlets or dimers. An up spin replacing a down spin destroys a singlet and gives rise to two domain-walls or solitons separating regions of dimerized order which are shifted in one lattice spacing with respect to each other. Each soliton carries a spin-1/2. Due to the spin-lattice coupling it is expected that the lattice solitons are driven by these magnetic solitons.

The soliton formation in spin-Peierls systems has been studied analytically by bosonization techniques applied to the spinless fermion model.<sup>16</sup> The coupling to the lattice is treated usually in the adiabatic approximation. The resulting field-theory formalism has led to important results, the most remarkable being the relation between the soliton width and the spin-Peierls gap,  $\xi \sim \Delta^{-1}$ .<sup>12</sup> Although this formalism has been extended to a Heisenberg model with competing NN and next-nearest-neighbor (NNN) antiferromagnetic interactions<sup>17,18</sup>, it presents some unsatisfactory features.

In the first place, there are some recent experimental results<sup>14</sup> for the soliton width in the IC phase in  $\text{CuGeO}_3$  indicating a disagreement with the theoretical prediction. Although there might be a contribution to

the soliton width coming from magnetic<sup>17</sup> or elastic<sup>18</sup> interchain couplings which would explain at least partially this disagreement, it is also possible that the differences could be due to several approximations involved in the bosonized field theory. One should take into account that these theories are valid in principle in the long wavelength limit, and the applicability of their results to real materials can not be internally assessed. Then, our first motivation to start a numerical study of the IC phase in spin-Peierls systems is to measure the importance of these approximations in the analytical approach.

In the second place, the field theory approach does not provide a detailed dependence of the magnitudes involved in terms of the original parameters of the microscopical models. For example, even for the simplest case<sup>12</sup> the expression obtained for the spin-wave velocity must be replaced by the exact one known from Bethe's exact solution of the Heisenberg chain. In this sense, numerical studies could give information about how the relevant magnitudes depend on the original parameters without further approximations.

With these motivations, in this article we want to initiate the study of the incommensurate phase in SP systems using numerical methods. These methods give essentially exact results for finite clusters, and they can be used to check various approximations required by the analytical approaches and the validity of their predictions. Besides, the numerical simulations provide a detailed information of the dominant magnetic and lattice states. In Section II we present the model considered and we study several features of the soliton formation in the IC phase using the Lanczos algorithm. In particular we analyze the effect of NNN interactions on the soliton width. In Section III we perform Monte Carlo simulations using the world line algorithm –which allows us to study larger chains than the ones accessible to the Lanczos algorithm– in order to reduce finite size effects.

## II. EXACT DIAGONALIZATION STUDY

The one-dimensional model which contains both the antiferromagnetic Heisenberg interactions and the coupling to the lattice is:

$$\mathcal{H} = J \sum_{i=1}^N (1 + (u_{i+1} - u_i)) \mathbf{S}_i \cdot \mathbf{S}_{i+1} + J_2 \sum_{i=1}^N \mathbf{S}_i \cdot \mathbf{S}_{i+2} + \frac{K}{2} \sum_{i=1}^N (u_{i+1} - u_i)^2 \quad (1)$$

where  $\mathbf{S}_i$  are the spin-1/2 operators and  $u_i$  is the displacement of magnetic ion  $i$  with respect to its equilibrium position. Periodic boundary conditions are imposed. The first term, which corresponds to the nearest neighbor (NN) interactions, contains the spin-lattice coupling in the adiabatic approximation. The second term contains

the AF NNN interactions, which were proposed in Refs. [ 19,20] to fit the experimental magnetic susceptibility data in CuGeO<sub>3</sub>. Several other properties of this material have been reasonably described using this model.<sup>21–23</sup> As in Ref. [ 19], we assume for simplicity that the lattice distortion does not affect the second neighbor interactions. In principle, the NNN interactions should be corrected by a term proportional to  $(u_{i+2} - u_i)$  which vanishes in the dimerized phase but not necessarily in the incommensurate phase. This correction should be important precisely in the region around a soliton. It is customary to introduce the frustration constant  $\alpha = J_2/J$ . The estimated value of  $\alpha$  in CuGeO<sub>3</sub> varies between 0.24 (Ref. [ 20]) and 0.36 (Ref. [ 19]). In this second case,  $\alpha$  is larger than the critical value  $\alpha_c \approx 0.2411$  above which in the absence of dimerization a gap opens in the excitation spectrum.<sup>24</sup>

Our purpose is to study numerically Hamiltonian (1) with exact diagonalization (Lanczos) techniques and by Monte Carlo simulations. In this latter case, in order to avoid the well-known sign problem due to the frustration, we will consider only the diagonal second neighbor interaction

$$\mathcal{H}_2^{zz} = J_2^z \sum_{i=1}^N S_i^z S_{i+2}^z, \quad (2)$$

instead of the isotropic NNN interactions (second term of Eq. 1).

It is quite apparent that the main numerical difficulty is related to the handling of the set of displacements  $\{u_i\}$ , which in principle can take arbitrary values to describe the various distortion patterns present in the dimerized and IC phases of the system. These displacements are calculated self-consistently by the following iterative procedure. First, we introduce the bond distortions defined as  $\delta_i = (u_{i+1} - u_i)$ . Then, the equilibrium conditions for the phononic degrees of freedom:

$$\frac{\partial \langle \mathcal{H} \rangle}{\partial \delta_i} + \lambda = 0 \quad (3)$$

lead to the set of equations:

$$J \langle \mathbf{S}_i \cdot \mathbf{S}_{i+1} \rangle + K \delta_i - \frac{J}{N} \sum_{i=1}^N \langle \mathbf{S}_i \cdot \mathbf{S}_{i+1} \rangle = 0, \quad (4)$$

which satisfies the constraint  $\sum_i \delta_i = 0$ . This constraint has been included in Eq. (3) through the corresponding Lagrange multiplier  $\lambda$ . The expectation values are taken with respect to the ground state of the system. The iterative procedure starts with an initial distortion pattern  $\{\delta_i^{(0)}\}$ , which in general we choose at random. At the step  $n$ , with a distortion pattern  $\{\delta_i^{(n-1)}\}$ , we diagonalize Hamiltonian (1) using the Lanczos algorithm and compute the correlations  $\langle \mathbf{S}_i \cdot \mathbf{S}_{i+1} \rangle$ . We replace these correlations in Eq. (4) and the new set  $\{\delta_i^{(n)}\}$  is

obtained. We repeat this iteration until convergence. Essentially the same procedure is followed in the quantum Monte Carlo algorithm, as it is discussed in Section III.

We have applied this exact diagonalization procedure to determine the distortion patterns in the 20 site chain at  $T = 0$ . In the first place we consider the case of  $S^z = 0$ . As mentioned above, this corresponds to a dimerized lattice, i.e.  $\delta_i = (-1)^i \delta_0$ . Notice that for this simple case, the equilibrium distortion amplitude  $\delta_0$  could be determined in an easier way by computing the energies of the spin part of Hamiltonian for a set of values of  $\delta_0$ . Then, adding the elastic energy and interpolating one obtains the minimum total energy. We have performed this calculation in order to check our iterative algorithm.

The results for  $\delta_0$  vs.  $K$ , for  $S^z = 0$ , are shown in Fig.1 for  $\alpha = 0.0, 0.2$  and  $0.4$ , and  $J_2^z = 0.2$ , and  $0.4$ . It can be seen that, as expected, for  $\alpha > 0$  the dimerized state is more favorable and this leads to a larger  $\delta_0$  for a given  $K$ . To a lesser extent this trend is also present for  $J_2^z > 0$ .

The dependence of  $\delta_0$  with  $K$  can be inferred from the scaling relation between the energy and the dimerization,  $E_0(\delta_0) - E_0(0) \sim \delta_0^{2\nu}$  (plus logarithmic corrections) with  $\nu = 2/3$ , in principle valid for  $\alpha < \alpha_c$  and small  $\delta_0$ .<sup>11,25,26</sup> Then, it is easy to obtain  $\delta_0 \sim K^{-3/2}$ , a relation which is approximately satisfied by our numerical data. The fact that  $\delta_0$  vanishes at a finite value  $\hat{K}$  of the elastic constant, is just a finite size effect. By diagonalizing chains of  $N = 12, 16$  and  $20$  sites, for  $\alpha = 0$ , we have verified that  $\hat{K}$  increases with the lattice size, as it can be seen in Fig. 2, and it should eventually diverge in the bulk limit.

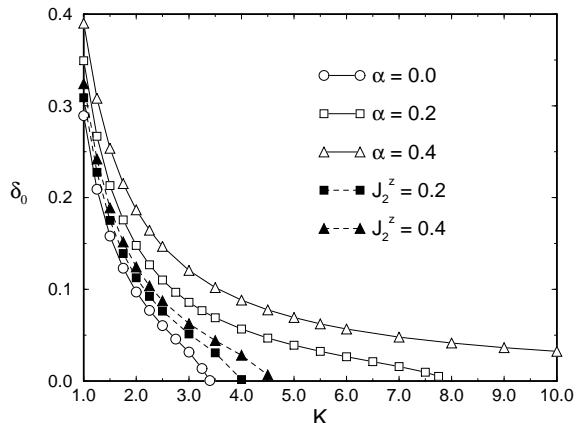


FIG. 1. Dimerization amplitude vs. elastic constant obtained by exact diagonalization in the 20 site chain,  $S^z = 0$ , for various values of  $\alpha = J_2/J$  and  $J_2^z$ .

Once we have determined the equilibrium distortion as a function of  $K$ , we are able to compute the singlet-triplet spin gap, defined as the following difference of ground state energies:

$$\Delta = E_{0,dim}(S^z = 1) - E_0(S^z = 0) \quad (5)$$

It is worth to emphasize that  $E_{0,dim}$  is the ground state

energy of the system for  $S^z = 1$  with the dimerization obtained for  $S^z = 0$  and the same set of parameters. The results of this calculation are shown in Fig. 3. Consistently with the larger  $\delta_0$  shown in Fig. 1, the gap increases with  $\alpha$ . The effect of  $J_2^z$  is much weaker than that of the isotropic second neighbor interaction which is not surprising since the 1D ground state magnetic structure, with a dominant dimerized state, has essentially a quantum (off-diagonal) origin. This small increase in  $\Delta$  for a given  $K$  is consistent with the small increase in  $\delta_0$  shown in Fig. 1. The corresponding scaling relation,  $\Delta \sim K^{-1}$ , obtained from the relation between the singlet-triplet gap and the dimerization,  $\Delta \sim \delta_0^{2/3}$ , is again reasonably satisfied by our numerical data.

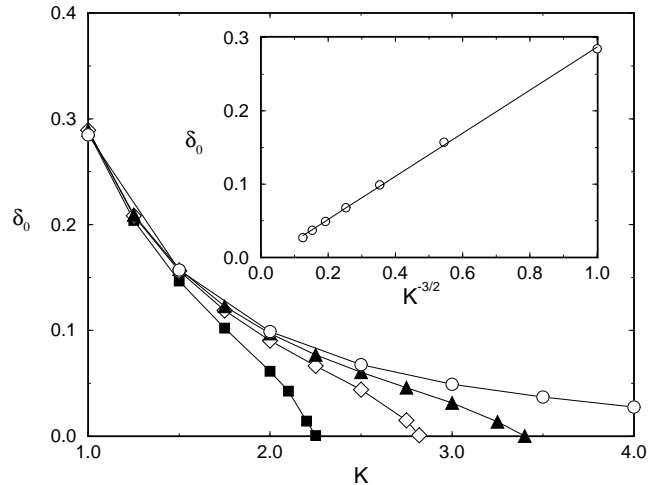


FIG. 2. Dimerization amplitude vs. elastic constant obtained by exact diagonalization for  $N = 12, 16, 20$  (solid squares, diamond and triangles, respectively) and Monte Carlo simulations for  $N = 64$  (open dots), with  $\alpha = 0$ . The inset shows the expected scaling behavior  $\delta_0 \sim K^{-3/2}$  for  $N = 64$ .

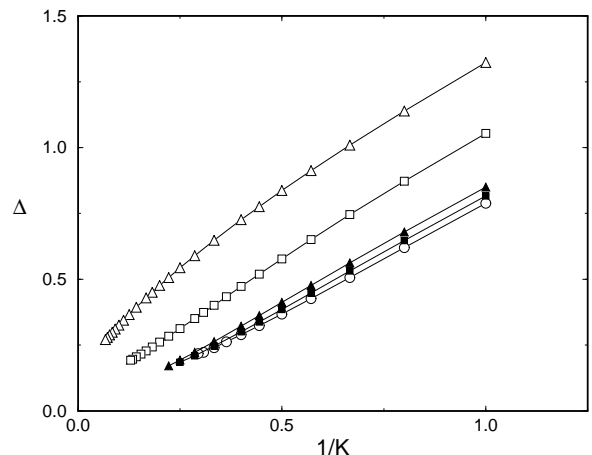


FIG. 3. Singlet-triplet gap vs. elastic constant obtained by exact diagonalization in the 20 site chain, for various values of  $\alpha$  and  $J_2^z$ . The symbols have the same meaning as in Fig. 1

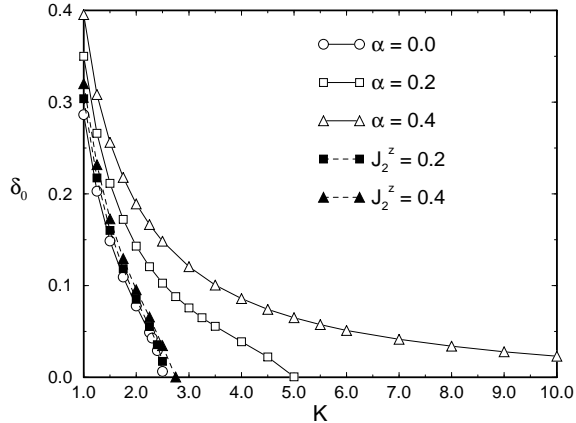


FIG. 4. Dimerization amplitude vs. elastic constant obtained by exact diagonalization in the 20 site chain,  $S^z = 1$ , for various values of  $\alpha$  and  $J_2^z$ .

We now consider the case of  $S^z = 1$ , which corresponds to the incommensurate region just above the dimerized-incommensurate transition. We have determined the distortion pattern for a 20 site chain using the iterative procedure described above. As discussed at the beginning of this section, the two solitons or domain walls separating dimerized regions are clearly distinguishable. (A typical pattern can be seen in Fig. 7.) The maximum distortion  $\delta_0$ , shown in Fig. 4, presents similar behavior as the one shown in Fig. 1 corresponding to  $S^z = 0$ . In particular, the fact that  $\delta_0$  vanishes at a finite  $K$  is again due to finite size effects.

In order to compute the soliton width, we use the following form to fit the numerically obtained distortion patterns:

$$\delta_i = (-1)^i \tilde{\delta} \tanh\left(\frac{i - i_0 - \frac{d}{2}}{\xi}\right) \tanh\left(\frac{i - i_0 + \frac{d}{2}}{\xi}\right), \quad (6)$$

which corresponds to modeling each soliton as an hyperbolic tangent, as obtained in the analytical approach to this problem.<sup>12</sup> The amplitude  $\tilde{\delta}$ , the soliton width  $\xi$ , and the soliton-antisoliton distance  $d$ , are the parameters determined by the numerical fitting. The amplitude  $\tilde{\delta}$  should be equal to the maximum distortion  $\delta_0$  defined above for well separated solitons, i.e.  $d \gg \xi$ . The main limitation of this calculation arises in the region where, for a given  $\alpha$ ,  $K$  is so large that the solitons have a substantial overlap in the 20 site chain, and the fitting function (6) is no longer appropriate. In this case, the elliptic sine should be used to describe the soliton lattice. This is the region where finite size effects are important, as it was discussed above with respect to Figs. 1 and 4. However, this situation is not directly relevant to experiment since in real materials the solitons are well-separated.<sup>14</sup>

We show in Fig. 5 the soliton width as a function of the gap  $\Delta$  for the 20 site chain, for the same values of

$\alpha$  and  $J_2^z$  as before. It can be seen that there is a linear dependence of the soliton width with the inverse of the gap. This behavior is consistent with the theoretical prediction:<sup>12</sup>

$$\xi = v_s / \Delta, \quad (7)$$

where  $v_s$  is the spin-wave velocity for  $\alpha < \alpha_c$ . It was recently shown that the relation (7), originally obtained for the unfrustrated chain,<sup>12</sup> is also valid in the presence of frustration.<sup>18</sup> For  $\alpha > \alpha_c$ ,  $\Delta$  contains a contribution from the frustration due to the presence of a gap even in the absence of dimerization.

A linear fitting of these curves in the region  $\xi > 2.5$  gives the slopes 1.87, 1.70 and 1.63, for  $\alpha = 0.0$ , 0.2 and 0.4 respectively. Recently, a numerical study<sup>27</sup> has proposed the law:  $v_s = \frac{\pi}{2}(1 - 1.12\alpha)$  in the bulk limit for  $\alpha < \alpha_c$ . From this law one gets  $v_s = 1.57, 1.22$ , for  $\alpha = 0.0$  and 0.2 respectively. We can observe that the slopes obtained by fitting the curves shown in Fig. (5) are systematically larger than these values of  $v_s$ . Besides, the effect of  $\alpha$  is weaker in the numerical data than that predicted by Eq. (7). For  $\alpha = 0.4 > \alpha_c \approx 0.2411$ , we have estimated  $v_s$  by fitting the excitation dispersion relation  $\varepsilon(k) = E_{0,dim}(S^z = 1, k) - E_0(S^z = 0, k = 0)$  with the law  $\varepsilon(k)^2 = \Delta^2 + v_s^2 k^2 + ck^4$  around  $k = 0$  and  $\delta_i = 0$ . For  $L = 20$  we obtained  $v_s = 0.707$ , a value which is also smaller than the slope of the curve  $\xi$  vs.  $1/\Delta$  for  $\alpha = 0.4$  in Fig. (5). This disagreement between the prediction obtained by the continuum bosonized theory and the numerical results could be due to the approximations involved in the former or to finite size effects present in the latter. The study of much larger lattices than those considered in this section will be done in the following section using quantum Monte Carlo simulations. On the other hand, for the case of  $J_2^z = 0.4$  the slope is actually larger ( $\approx 2.1$ ) than the value obtained for the Heisenberg chain with NN interactions only. This effect is opposite to that of the isotropic NNN interactions and it will be further discussed in the next section.

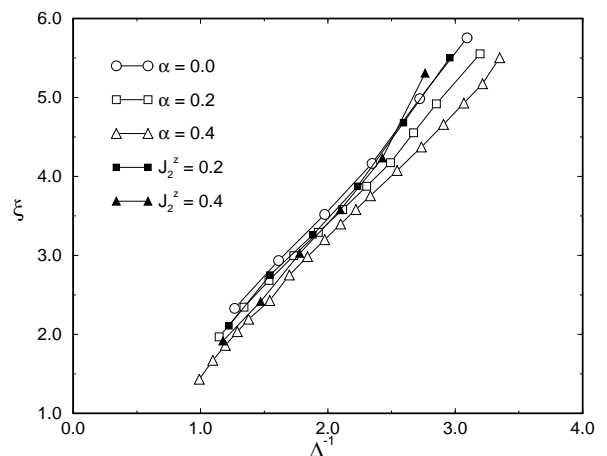


FIG. 5. Soliton width vs. singlet-triplet spin gap obtained by exact diagonalization in the 20 site chain,  $S^z = 0$ , for various values of  $\alpha$  and  $J_2^z$ .

### III. MONTE CARLO SIMULATIONS

In order to treat longer chains than those considered in the Lanczos diagonalization study of the previous section, we have implemented a world-line Monte Carlo algorithm<sup>28</sup> suited to this problem. The partition function is re-expressed as a functional integral over worldline configurations, where the contribution on each imaginary-time slice is given by the product of the two-site evolution matrix elements,

$$W_{i,i+1}(\tau) = \langle S_{i,\tau}^z S_{i+1,\tau}^z | e^{-\Delta\tau J_i \mathbf{S}_i \cdot \mathbf{S}_{i+1}} | S_{i,\tau+\Delta\tau}^z S_{i+1,\tau+\Delta\tau}^z \rangle$$

where  $J_i = J(1 + \delta_i)$ . These matrix elements are the Boltzmann weights associated with a bond  $(i, i+1)$  in a time step  $\Delta\tau = 1/mT$  in the Trotter direction, where  $T$  is the temperature and  $m$  is the Trotter number. Since the exchange couplings depend on the lattice displacements, these matrix elements are site dependent.

We implemented the algorithm with the addition of a dynamic minimization of the free energy with respect to the lattice displacements. Starting from a given initial configuration (random distribution of spins and a dimerized pattern for the lattice displacements) we typically considered  $2 \times 10^3$  sweeps for thermalization. During the next  $4 \times 10^3$  sweeps we measured the derivative of the magnetic free energy, which, in the limit of  $T \rightarrow 0$ , is given by

$$\frac{\partial \mathcal{F}_M}{\partial \delta_i} = J \langle \langle \mathbf{S}_i \cdot \mathbf{S}_{i+1} \rangle \rangle_T. \quad (8)$$

Leaving 3 sweeps between each measurement for decorrelation this produces  $10^3$  independent values to obtain the thermal average. With this free-energy gradient we corrected the displacements according to (4) and repeated the procedure, including the  $2 \times 10^3$  sweeps for thermalization since the spins have to accommodate to the new lattice distortions. Once the displacement pattern is stabilized within statistical fluctuations —we typically considered  $\sim 150$  iterations, see Fig. 6— we performed measurements of several quantities. For this we obtained 100 independent groups of  $10^3$  measurements each, following the same procedure as described above, *i.e.*, i) thermalization, ii) measurements of  $\frac{\partial \mathcal{F}_M}{\partial \delta_i}$  and observables, and iii) correction of the displacement pattern due to statistical fluctuations.

In our calculations we considered chains of 64 sites with periodic boundary conditions and a temperature  $T = 0.05J$ . We checked that this value is low enough to study ground-state properties by comparison with measurements at even lower temperatures. On the other hand, at higher temperatures the soliton is not observed and there is no definite pattern of lattice displacements. We took  $m = 80$  for the Trotter number, which is large enough to reproduce the Lanczos results on smaller chains (see Fig. 2). For some particular quantities like the energy gap, which require more precision, we considered also  $m = 160$ . In addition, comparison with results

for a longer chain with  $N = 128$  indicates that in the parameter range of our calculations the Monte Carlo results have no sizeable finite-size effects.

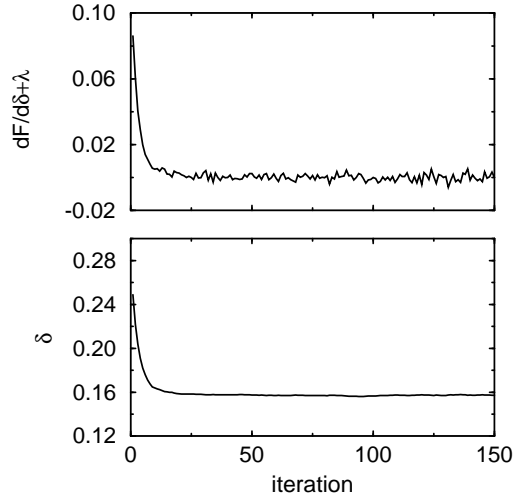


FIG. 6. Minimization of the free energy for a uniform dimerized chain. We plot the derivative of the free energy and the parameter  $\delta$  along the successive iterations.

In Fig. 2 we show the Monte Carlo results for the homogeneous dimerization of the 64 site chain in the  $S^z = 0$  subspace as a function of the elastic constant  $K$ , together with the Lanczos results for smaller chains. Notice that in the parameter range considered the 64 site chain does not have the finite size effects present for smaller chains, namely, the vanishing of  $\delta_0$  for finite values of  $K$ . The inset shows the expected scaling behavior  $\delta \propto K^{-3/2}$  discussed in the previous section. As a further check, we have also reproduced the scaling behavior of the energy gain  $E_0(\delta_0) - E_0(0)$  and gap with  $\delta_0$  with a measured exponent  $\nu = 2/3$  within statistical errors.

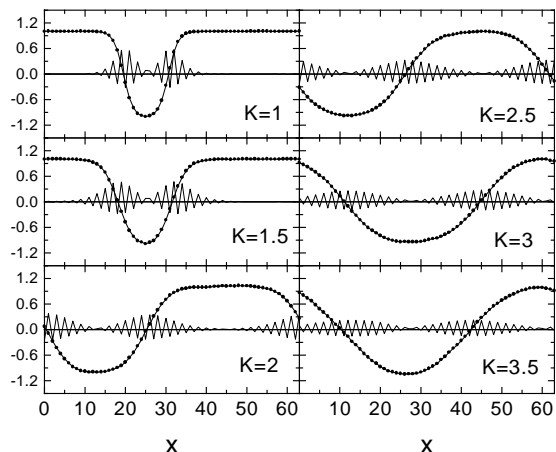


FIG. 7. Lattice distortion patterns and local magnetizations of the 64 site chain obtained by Monte Carlo, for  $S^z = 1$  and different values of  $K$ . In every panel the maximum lattice distortion is normalized to one, so that they cannot be directly compared.

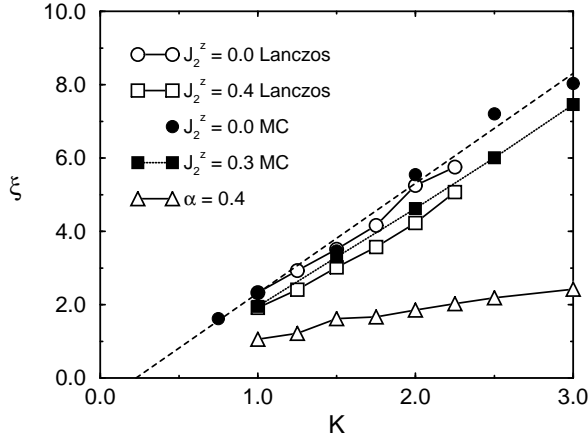


FIG. 8. Soliton width vs. elastic constant  $K$  obtained by Monte Carlo simulations in the 64 site chain for  $J_2^z = 0.0$  and  $0.3$ , together with Lanczos results for the 20 site chain,  $J_2^z = 0.0$  and  $0.4$ , and  $\alpha = 0.4$ . The dashed line corresponds to a linear fit to the Monte Carlo results for  $J_2^z = 0$ .

The soliton structure in the subspace with  $S^z = 1$  is given in Fig. 7, where we plot the displacement envelope  $\tilde{\delta}_i = (-)^i \delta_i$  and the local magnetization  $\langle S_i^z \rangle$ , for different values of the elastic constant  $K$ . Notice that the displacements are normalized by their maximum values (shown in Fig. 2) and the local magnetization by the classical value  $S = 1/2$ . Consequently, the size of lattice distortions in different panels cannot be directly compared. For small values of  $K$  there is a well defined soliton-antisoliton structure in the distortion pattern, with the associated local magnetization following a staggered order. There is a net  $1/2$  spin density near each domain wall, which makes the excess  $S^z = 1$ . As in the previous section, we fitted a two-soliton solution (6), with  $\tilde{\delta}_0 = 1$  because of the normalization adopted. The results for the soliton width  $\xi$  are shown in Fig. 8. For increasing values of  $K$  the soliton width grows until the displacement profile resembles a sine law (see Fig. 7). This sinusoidal pattern is typical of the soliton lattice, observed for large values of  $S^z$ . It can be seen that the scaling  $\xi \sim K$  obtained in [12] is well reproduced in the whole parameter range considered, as indicated by the linear fit to the data (dashed line). This figure shows that the soliton width for  $J_2^z = 0.3$  also presents a linear dependence with  $K$ . These features observed in the 64 site chain are qualitatively similar to those present in the 20 site chain as determined by exact diagonalization. Besides, it can be seen in this figure that the reduction of  $\xi$  is much stronger when the isotropic NNN is taking into account.

We have performed a simple study on the soliton-antisoliton interaction. For this study we fixed the distortion pattern to the law (6) with the previously fitted

value of  $\xi$ , and considered increasing values of  $d$ . For small  $K$  ( $\leq 2J$ ) we found that the total energy becomes a constant (within statistical fluctuations) when  $d \geq 4\xi$ , which implies that the soliton-antisoliton pairs shown in the left panels of Fig. 4 are not interacting. This was confirmed by allowing the lattice distortion to evolve starting from a pattern like (6) with an initial separation larger than  $d$ , which produces the same result for  $\xi$  and the total energy.

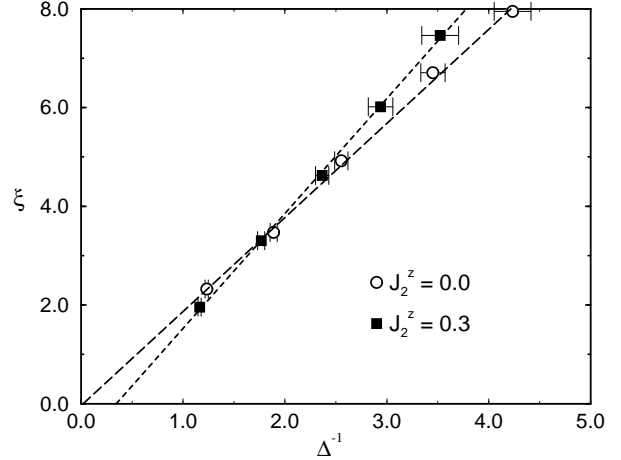


FIG. 9. Soliton width vs. inverse of singlet-triplet gap obtained by Monte Carlo simulations for  $J_2^z = 0.0$  and  $0.3$ . The horizontal error bars give the estimated error in the determination of the gap  $\Delta$ .

Next, we study the behavior of the soliton width  $\xi$  with the spin-Peierls gap  $\Delta$ . That is, we compare the quantity  $\xi$  that characterizes the  $S^z = 1$  soliton state, with the singlet-triplet excitation gap  $\Delta$  above the dimerized  $S^z = 0$  ground state. As shown in Fig. 9, these two quantities are inversely related to each other, as discussed in the previous section. The slope of the linear fit is 1.9, very close to the value 1.87 obtained by exact diagonalization of the 20 site chain in the previous section. This result confirms the disagreement between the numerical results with the analytical prediction pointed out in Section II. Also shown in Fig. 9 are the results for  $J_2^z = 0.3$ . A linear fit to these results leads to a slope  $\approx 2.3$ , i.e. larger than the value corresponding to  $J_2^z = 0.0$ . This increase of the slope between  $\xi$  and  $\Delta^{-1}$  is consistent with the result obtained for the 20 site lattice by exact diagonalization and  $J_2^z = 0.4$ . This behavior should be contrasted with the *reduction* of the slope found for the isotropic NNN interaction. A possible explanation of this behavior could be the following. As discussed in the previous section, the term  $\mathcal{H}_2^{zz}$  leads to a smaller increase of the spin gap than the fully isotropic NNN interaction. On the other hand, the Ising interaction could be more effective in punishing the excess  $\langle S^z \rangle$  which appears around a soliton leading to a smaller reduction of the soliton width than the one caused by the isotropic term, as it can be seen in Fig. 8. A more detailed study of the Hamiltonian in the presence

of the term of  $\mathcal{H}_2^z$  is clearly necessary to fully understand this behavior.

Finally, it is possible to estimate the critical value of the magnetic field at zero temperature. By adding a Zeeman term to the Hamiltonian (1),  $-g\mu_B S^z H$  ( $\mu_B$ : Bohr's magneton),  $H_{cr}$  may be calculated as:

$$H_{cr} = E_0(S^z = 1) - E_0(S^z = 0) \quad (9)$$

in units of  $g\mu_B$ .  $E_0(S^z = 1)$  is the ground state energy of (1), and then  $H_{cr} < \Delta$ , which is the value expected of a gapped system in the absence of magneto-elastic coupling. The behavior of  $H_{cr}$  as a function of  $\Delta$  is shown in Fig. 10 for the 64 site chain,  $\alpha = J_2^z = 0.0$ , and for the 20 site chain,  $\alpha = J_2^z = 0.4$ . It is apparent a linear dependence over all the range studied, which is in agreement with the mean-field prediction<sup>3,11</sup>,  $H_{cr} \approx 0.84\Delta$ . However, we obtain a coefficient considerable smaller,  $H_{cr}/\Delta \approx 0.47$ , almost independent of  $\alpha$ . This value is also smaller than twice the soliton formation energy calculated in Ref. [12]. The finite value at the origin of the curves corresponding to  $\alpha = J_2^z = 0.4$  is a finite size effect.

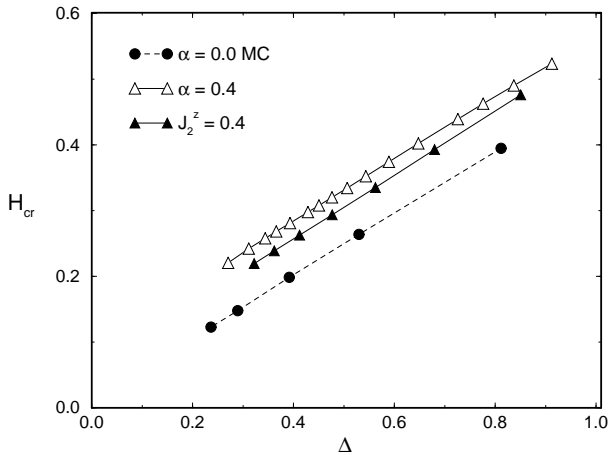


FIG. 10.  $H_{cr}$  vs. spin gap obtained by Monte Carlo in the 64 site chain for  $\alpha = J_2^z = 0.0$  and by exact diagonalization in the 20 site chain, for  $\alpha = J_2^z = 0.4$ .

#### IV. CONCLUSIONS

In this article we have analyzed the magnetic soliton lattice in the incommensurate phase of spin-Peierls systems using numerical methods. There is a remarkable agreement between the results obtained by exact diagonalization using the Lanczos algorithm and those obtained by quantum Monte Carlo with the world-line algorithm. The relations among various features of the solitons and magnetic properties of the system have been determined and compared with analytical results. Our starting point is a microscopical model proposed to describe several properties of  $\text{CuGeO}_3$ , consisting of a 1D AF Heisenberg model with nearest and next-nearest neighbor interactions.

In the first place we have not detected any crossover in the behavior of the quantities examined as  $\alpha$ , the ratio of NNN to NN interactions, becomes greater than  $\alpha_c$  at least for the small chains considered. That is, there are only smooth changes as  $\alpha$  varies between 0.0 and 0.4. The most important effect of the competing NNN interaction is a *reduction* of the soliton width  $\xi$  as a function of the inverse of the singlet-triplet spin gap  $\Delta$ . Furthermore, the effect of the diagonal term (2) is much less important and in some cases even qualitatively different to that of the isotropic NNN term.

Although several functional forms predicted by continuum analytical theories have been confirmed by our numerical data, there are some important quantitative differences. The most important disagreement between our numerical results and the analytical predictions is related to the coefficient in the relation  $\xi \sim \Delta^{-1}$ , i.e. we have obtained a systematically higher value than the theoretical value which is the spin-wave velocity. The estimated value of  $H_{cr}/\Delta$  is also noticeable smaller than the mean-field result and slightly smaller than the prediction of bosonized field theory. The relevance of these numerical results to real SP materials, such as  $\text{CuGeO}_3$  and the recently discovered  $\text{NaV}_2\text{O}_5$ ,<sup>29</sup> has to be determined experimentally.

The numerical procedures developed in this article could be applied to the study of several other properties of the incommensurate phase of spin-Peierls systems, such as the static magnetization as a function of the magnetic field (recently measured in  $\text{CuGeO}_3$  by Fagot-Revurat *et al.*<sup>15</sup>) and the order of the transition from the dimerized to the incommensurate phases.<sup>9</sup>

<sup>1</sup> F. D. M. Haldane, Phys. Rev. Lett. **50**, 1153 (1983).

<sup>2</sup> For a recent review see *Physics Today*, Search and Discovery, pg. 17 October 1996.

<sup>3</sup> E. Pytte, Phys. Rev. B **10**, 2309 (1974).

<sup>4</sup> M. Hase, I. Terasaki and K. Uchinokura, Phys. Rev. Lett. **70**, 3651 (1993).

<sup>5</sup> L. P. Regnault *et al.*, Phys. Rev. B **53**, 5579 (1996).

<sup>6</sup> J.-L. Lussier *et al.*, J. Phys. Condens. Matter **7**, 325 (1995).

<sup>7</sup> M. C. Cross, Phys. Rev. B **20**, 4606 (1979).

<sup>8</sup> M. Hase *et al.*, Phys. Rev. B **48**, 9616 (1993).

<sup>9</sup> P. H. M. van Loosdrecht *et al.*, Phys. Rev. B **54**, 3730 (1996).

<sup>10</sup> M. Fujita and K. Machida, J. Phys. Jpn **53**, 4395 (1984).

<sup>11</sup> M.S. Cross and D.S. Fisher, Phys. Rev. B **19**, 402 (1979).

<sup>12</sup> T. Nakano and H. Fukuyama, J. Phys. Jpn **49**, 1679 (1980).

<sup>13</sup> A. I. Buzdin, M. L. Kubic, and V. V. Tugushev, Solid State Commun. **48**, 483 (1983).

<sup>14</sup> V. Kiryukhin *et al.*, Phys. Rev. Lett. **76**, 4608 (1996); V. Kiryukhin *et al.*, Phys. Rev. B **54**, 7269 (1996).

<sup>15</sup> Y. Fagot-Revurat *et al.*, Phys. Rev. Lett. **77**, 1861 (1996).

- <sup>16</sup> I. Affleck, *Fields, Strings and Critical Phenomena*, edited by E. Brézin and J.Zinn-Justin (North-Holland, Amsterdam, 1990), pg. 563.
- <sup>17</sup> J. Zang, S. Chakravarty and A.R. Bishop, cond-mat/9702185.
- <sup>18</sup> A. Dobry and J. Riera, (to be published).
- <sup>19</sup> J. Riera and A. Dobry, Phys. Rev. B **51**, 16098 (1995).
- <sup>20</sup> G. Castilla, S. Chakravarty and V.J. Emery, Phys. Rev. Lett. **75**, 1823 (1995).
- <sup>21</sup> S. Haas and E. Dagotto, Phys. Rev. B **52**, 14396 (1995).
- <sup>22</sup> J. Riera and S. Koval, Phys. Rev. B **53**, 770 (1996).
- <sup>23</sup> D. Poilblanc *et al.*, Phys. Rev. B, to appear (1997).
- <sup>24</sup> K. Okamoto and K. Nomura, Phys. Lett. A **169**, 433 (1992).
- <sup>25</sup> G. Spronken, B. Fourcade, and Y. Lépine, Phys. Rev. **33**, 1886 (1986), and references therein.
- <sup>26</sup> Numerical calculations indicate that this relation still holds with an exponent  $\nu$  close to  $2/3$ , for  $\alpha > \alpha_c$ , at least for not too small  $\delta_0$  and  $\alpha < 1/2$ ; M. Laukamp and J. Riera, (to be published).
- <sup>27</sup> A. Fledderjohann and C. Gros, cond-mat/9612013.
- <sup>28</sup> J. E. Hirsch *et al.*, Phys. Rev. B **26**, 5033 (1982).
- <sup>29</sup> M. Isobe and Y. Ueda, J. Phys. Soc. Jpn. **65**, 1178 (1996); M. Weiden, R. Hauptmann, C. Geibel, F. Steglich, M. Fischer, P. Lemmens and G. Güntherodt, preprint cond-mat/9703052.